Time-resolved studies of NO_2 photoinitiated unimolecular decomposition: step-like variation of $k_{uni}(E)$ ☆

G.A. Brucker, S.I. Ionov, Y. Chen [1] and C. Wittig
Department of Chemistry, University of Southern California, Los Angeles, CA 90089-0482, USA

Received 20 March 1992; in final form 14 April 1992

Time-resolved, subpicosecond-resolution measurements of NO_2 photoinitiated unimolecular decay rates are reported for jet-cooled samples in the vicinity of the dissociation threshold. The molecules are excited by 385–400 nm tunable subpicosecond pulses to the $^2B_2$ electronic state which is very strongly mixed with the $^2A_1$ ground electronic state. Subsequent decomposition is probed by a 226 nm subpicosecond pulse which excites LIF in the NO product. When changing the amount of energy in excess of the dissociation threshold, a step-like increase of the reaction rate versus energy is observed.

1. Introduction

The photoinitiated unimolecular reaction of NO_2 is presently the only documented case in which a stable *triatomic* can be excited optically via an allowed one-photon transition to levels that lie above the reaction threshold and that have predominantly ground electronic state character. It is known that near-infrared, visible, and ultraviolet photons excite NO_2 into a region of strong mixing between the $^2A_1$ ground state and the $^2B_2$ electronically excited state [1–12]. Moreover, excitation between 250 and 398 nm results in NO_2 decomposition to NO and O in their electronic ground states, i.e., $^2\Pi_\Omega$ and ^3P_J, respectively, where Ω and J label fine structure levels [5–10]. Energies above reaction threshold, which is determined to be $D_0 = 25130.6$ cm^{-1} [7,13], are spectroscopically accessible over a broad, continuously tunable range, and the NO($X\,^2\Pi$) molecular fragment is particularly amenable to sensitive, state-selective detection.

Recent spectroscopic studies have successfully assigned NO_2 vibrational levels of the ground electronic state up to 10000 cm^{-1} [3], and the density of vibronic levels on the strongly coupled $^2A_1$ and $^2B_2$ electronic surfaces has been experimentally estimated in the region 16500–18500 cm^{-1} [4]. Moreover, spectra of extremely cold (≈ 1 K) expansion-cooled samples have been taken in the region just below D_0 [9]. Such data provide quantitative experimental assessments of vibronic and rovibronic level densities near D_0, facilitating comparisons between theoretical predictions and measured reaction rates. These features make NO_2 unimolecular decay rates very attractive for scrupulous experimental examinations.

Several groups have examined NO_2 photofragmentation in detail, reporting center-of-mass (CM) kinetic energy distributions obtained from time-of-flight (TOF) analyses [14], and state selective product detection of O(^3P_J) [8,9] as well as NO($X\,^2\Pi$) [7,10]. In a pioneering study by Troe and co-workers, high pressure samples containing NO_2 were photolyzed at a number of different ultraviolet wavelengths, yielding the variation of decomposition lifetime versus the photon energy of the photolyzing light [15]. These results were analyzed using reaction rate theories, and in fact have been central to the development and refinement of such theories

Correspondence to: C. Wittig, Department of Chemistry, University of Southern California, Los Angeles, CA 90089-0482, USA.
☆ Research supported by the US Army Research Office.
[1] Present address: Department of Chemistry, University of California, Berkeley, CA 94720, USA.

0009-2614/92/$ 05.00 © 1992 Elsevier Science Publishers B.V. All rights reserved.

[16–18]. On the negative side, interpretations of experimental results on NO_2 photochemistry are not always straightforward, due to the molecule's complex electronic structure. There is a conical intersection between the $^2A_1$ ground state and the lowest electronically excited $^2B_2$ state [11,12] and the use of a single effective potential, in dynamics studies for example, cannot be justified a priori.

Difficulties notwithstanding, NO_2 is a scientifically and technologically important species and although several measurements of its photochemistry have been carried out in the region just above D_0, there has been no report to date of direct measurements of decomposition lifetimes. Thus, we have carried out time-resolved, subpicosecond-resolution measurements of photoinitiated NO_2 reaction rates using expansion-cooled samples. These are the first direct measurements of the reaction rates for this system. The rates show an essentially monotonic increase with energy, and are consistent with the step-like variation of k_{uni} versus E predicted by transition state theories. In this communication, we report the essence of these measurements. These results constitute an important complement to the detailed unimolecular reaction rate studies carried out for NCNO [19] and CH_2CO [20].

2. Experimental

The experimental arrangement is shown schematically in fig. 1. The main parts are: (i) a dual-jet mode-locked dye laser (Coherent 702-1), synchronously pumped by the frequency-doubled output of (ii) an actively mode-locked Nd:YAG laser (Spectron SL 903), (iii) two dye amplifiers pumped by (iv) a regenerative Nd:YAG amplifier (Continuum RGA 69-10), and (v) a vacuum chamber equipped with a pulsed nozzle, quadrupole mass spectrometer and accessories for monitoring LIF. The mode-locked

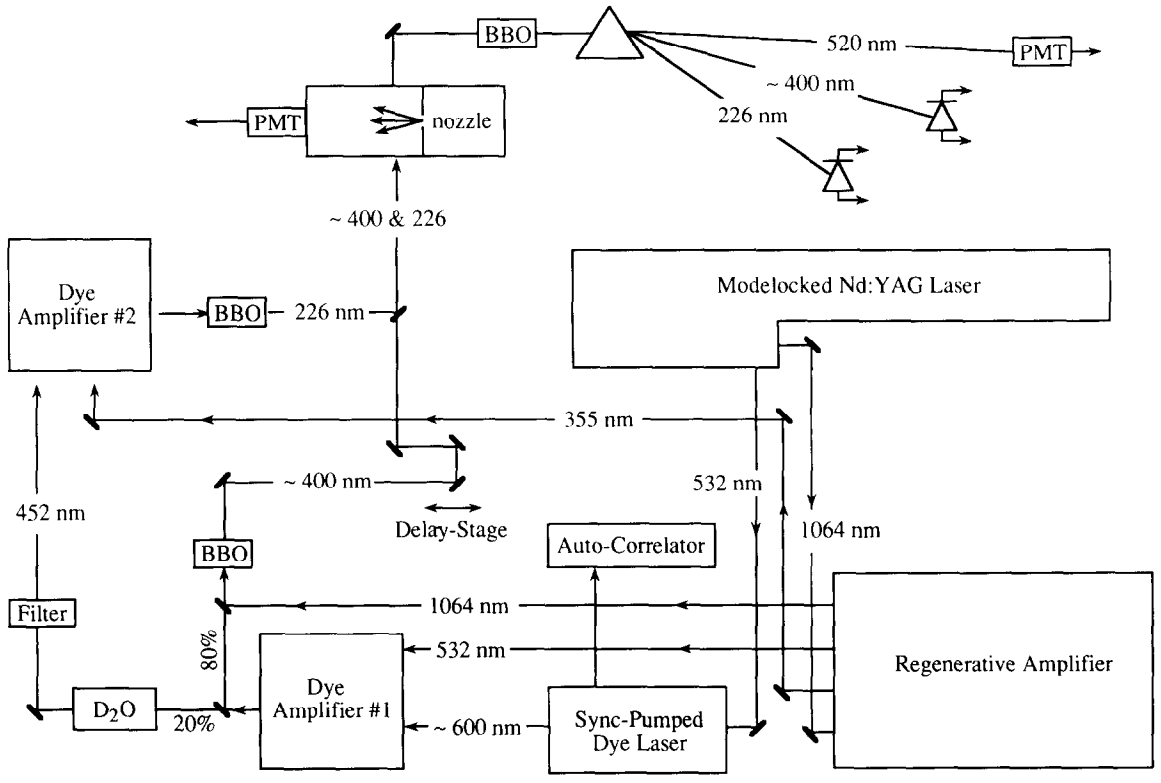

Fig. 1. Schematic diagram of the experimental arrangement.

Nd:YAG laser with a CAMAC ML 4000 mode-locker generates a train of 100 ps pulses at 76 MHz; typical average power is 20 W at 1064 nm. A 5% portion of this radiation is used for seeding the regenerative amplifier, the remaining 95% is frequency doubled in a 12 mm LBO crystal producing about 2 W of 532 nm radiation for dye laser pumping.

Table 1 presents the combinations of gain and saturable absorber dyes used in the dual-jet dye oscillator and first amplifier. Using a single-plate birefringent filter (BRF) as a tuning element, 250–500 fs pulses tunable from 575 to 645 nm with $\approx$40–70 cm^{-1} spectral bandwidth are obtained from the mode-locked dye laser. The shortest pulses are observed on the red side of the covered spectral range. Replacing the single-plate BRF by a double-plate BRF results in the bandwidth narrowing to $\approx$30% of its original value. This narrowing is accompanied by broadening of the pulsewidth. Although 300 mW is obtained at the exit of the dual-jet dye laser, only half of this is used for successive amplification in order to minimize pulse broadening.

The output pulse train from the dye laser is amplified in a three-stage amplifier (Continuum PTA-60). The amplifier is longitudinally pumped at 10 Hz by the second harmonic of the RGA which typically provides 30 mJ, 80 ps pulses at 532 nm. There is a solid state saturable absorber (table 1) positioned between the first and the second amplification stages for reducing pulse broadening. The amplified dye laser pulse, which reaches 2 mJ without noticeable broadening, is divided into two beams by a broadband beam-splitter. The first beam, with $\approx$80% of the energy, is spatially matched using a telescope and then combined on a dichroic mirror with a 1064 nm, 50 mJ beam from the RGA. These beams are mixed in a BBO crystal producing $\approx$200 μJ of sum frequency radiation tunable from 373 to 402 nm. No significant broadening is observed in this near-UV pulse, as ascertained from its cross-correlation with the dye laser fundamental. The cross-correlation is measured by sum-frequency generation in a 150 μm BBO crystal. The near-UV pulse is used to excite NO_2 molecules over the dissociation threshold causing their unimolecular decomposition.

The remaining 20% of the amplified dye laser fundamental is focused by a 10 cm f.l. lens into a D_2O cell producing a white continuum. To avoid boiling, the heavy water is constantly stirred by a magnetic stirrer. Vertically polarized 452 nm radiation ($\approx$1 nJ, 6 nm bandwidth) is selected from the continuum by a Corning 5-57 glass filter followed by a Glan–Taylor polarizer and an interference filter. These components are positioned behind an 8 cm f.l. lens which recollimates the light exiting the D_2O cell. Autocorrelation traces of the filtered continuum show $\approx$50% temporal broadening of the 452 nm pulses as compared to the dye laser fundamental. We believe that this broadening is due to the interference filter. The 452 nm radiation is amplified in a second three-stage dye amplifier transversely pumped by 45 mJ, 355 nm pulses from the RGA. Coumarin 460/MeOH dye solutions are used in the first and final stages. In order to minimize ASE, a different dye, coumarin 440/MeOH, is used in the second stage. The dye concentrations are adjusted in each stage to satisfy

Table 1
Gain and saturable absorber (S/A) dyes used in the dual-jet dye oscillator and the first dye amplifier.

Wavelength	Oscillator dyes		Amplifier	
(nm)	gain	saturable absorber	gain dyes	solid-state saturable absorber [a]
575–595	Rh590(Cl)	DODCI/DQOCI	Rh610	RG610
595–605	Rh590(Cl)	DODCI/DQTCI	kiton red (H_2O) or SRh640 (MeOH)	RG630
605–618	kiton red	DQTCI	DCM (MeOH) or SRh640 (MeOH)	RG645
618–645	kiton red/SRh640	DQTCI	DCM (MeOH)	RG665

[a] Solid state saturable absorber: long-pass, Schott-glass filter located at the beam focal point between the first and second stages of amplification to reduce pulse broadening.

two contradictory criteria: maximum power and minimum pulse reshaping due to saturation. The amplified 452 nm beam ($\approx$250 μJ) is frequency doubled in a 150 μm long BBO crystal. The resulting 226 nm laser pulse is used to probe NO via LIF using the γ system.

After passing through a computer-controlled delay stage (Aerotech ATS100) the pump beam is combined with the probe radiation on a dichroic mirror and collinearly focused by a 30 cm f.l. lens into a vacuum chamber pumped to 10^{-6} Torr. The chamber is equipped with a pulsed nozzle (250 μs duration, 500 μm dia. orifice), a quadrupole mass spectrometer for monitoring the beam intensity, a PMT (Hamamatsu 943-02) and collecting optics for LIF measurements. The collinear laser beams intersect the supersonic jet $\approx$40 nozzle diameters downstream from the nozzle. A 3% NO_2/He gas mixture is prepared in situ by blowing 1 atm of He over an NO_2 sample frozen at -28°C. A 760 Torr stagnation pressure is kept throughout the measurements. The NO_2 sample (Matheson, 99.5%) is purified prior to each set of experiments by bubbling O_2 through the liquid at 0°C followed by several freeze–pump–thaw cycles. The prepared sample is kept under 1 atm of oxygen between experimental runs in order to shift the $NO_2 \leftrightarrow NO + \frac{1}{2}O_2$ equilibrium towards NO_2. To further minimize NO_2 decomposition, the nozzle interior is coated with Teflon and the portion of the gas system between the NO_2 bath and the nozzle is kept at -20°C.

The NO LIF signal is preamplified, digitized and collected in an IBM AT computer simultaneously with both pump and probe pulse energies and a pump–probe cross-correlation signal. The cross correlation is obtained by difference frequency generation in a 100 μm BBO crystal which is positioned shortly after the chamber. The pump, probe and difference frequency radiations are separated in a 60° quartz prism and detected by two UV-grade photodiodes and a PMT, respectively.

3. Results

When the pump radiation wavelength is below 397.9 nm, NO fragments deriving from the photodecomposition of expansion-cooled NO_2 are observed by LIF following the pump pulse. Results obtained with room temperature samples will be described elsewhere. No decomposition is detected at $\lambda_{pump} \geq 398$ nm. This observation is in good agreement with the reported threshold for NO_2 decomposition, 25130.6 cm^{-1} [7,13]. Typical experimental scans of NO LIF signal versus the delay between the pump and probe pulses are shown in fig. 2. There are typically 300–500 data points in each trace, and each of the points represents an average over 20 laser shots and is normalized to the pump and probe energies. Also shown in the figure are the corresponding pump–probe cross correlations which have been recorded by difference-frequency generation simultaneously with obtaining the LIF signal. We have verified experimentally that the NO LIF signal is a linear function of both pump and probe laser energies and that the experimentally determined decay rates (see below) are independent of the pump energy. Therefore, the observed decomposition of NO_2 results from a one-photon process.

The experimental time dependencies are fit assuming single exponential NO production after the excitation event:

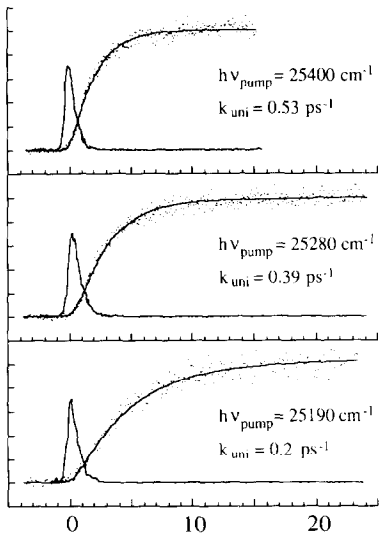

Fig. 2. NO LIF measured as a function of the pump–probe delay time for the indicated excitation conditions. Also shown are the corresponding cross correlations between the pump and probe pulses. The experimental points are fitted assuming single exponential decay as described in the text.

$$S(t) \propto \int_{-\infty}^{t} \mathrm{d}s\, R(s)\{1-\exp[-k_{\mathrm{uni}}(t-s)]\}\,, \qquad (1)$$

where

$$R(s) = \int_{-\infty}^{\infty} \mathrm{d}t\, I_{\mathrm{pump}}(t) I_{\mathrm{probe}}(t-s)\,, \qquad (2)$$

$R(s)$ is the experimentally measured cross correlation between the pump and probe pulses and k_{uni} is the unimolecular reaction rate under consideration. Fits of the experimental data by the above convolution are shown as solid lines in fig. 2. As seen from the figure, the assumption of a single exponential decay provides good agreement with the data. The small discrepancies between the experimental results and the simulations are not serious. We note that the spectral bandwidth of the pump pulse, i.e., 20–80 cm^{-1}, results in excitation of a number of molecular eigenstates, as discussed in the next section. Since the state-to-state dissociation rate is expected to fluctuate considerably [21], modest deviations from single exponential decay are not surprising.

The NO_2 dissociation rates obtained from the experimental delay time dependencies described above are presented in fig. 3. Every point in the figure is an average of 8 to 16 rates, each obtained from independent scans at specific excitation wavelengths.

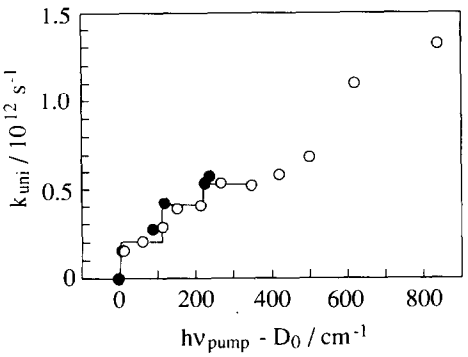

Fig. 3. NO_2 unimolecular decay rate versus energy in excess of reaction threshold. Closed circles are for the double-plate BRF which provides ≈ 1.5 ps fwhm cross correlations and 20–30 cm^{-1} bandwidth. Open circles are for the single-plate BRF; 0.5–0.9 ps fwhm cross correlations; 40–80 cm^{-1} bandwidth.

Statistical uncertainties, i.e., standard deviations, are small, generally lying within the circles shown in fig. 3. It should be noted that independent measurements have been carried out for several excitation wavelengths near the reaction threshold with either one or two birefringent filters in the mode-locked dye oscillator. As discussed in the previous section, the single-plate BRF provides better time resolution, i.e., 500 to 900 fs cross correlation fwhm, with lower spectral resolution of ≈ 40–80 cm^{-1}, as compared to the double-plate BRF, which provides ≈ 1.5 ps cross correlations and 20–30 cm^{-1} spectral resolution. The experimental points obtained with the single- and double-plate BRFs are presented by closed and open symbols, respectively.

One aspect of the results presented in fig. 3 is noteworthy. Namely, k_{uni} versus $h\nu_{\mathrm{pump}}$ is not a smooth ascending function, as is often the case for unimolecular decompositions. For example, the rate rises abruptly to $\approx 1.6\times10^{11}$ s^{-1} at threshold and then rises only moderately in the range 0–100 cm^{-1}. The rate exhibits another steep rise to $\approx 4\times10^{11}$ s^{-1} for excess energies near 100 cm^{-1} and then does not change in the range 120–210 cm^{-1}. At 220 cm^{-1} the rate climbs to $\approx 5.5\times10^{11}$ s^{-1} and then flattens again in the range 240–350 cm^{-1}. These step-like rises cannot be dismissed as a S/N problem, i.e. each data point is the result of considerable signal averaging and is reproducible. In similar experiments carried out in our laboratory with room temperature samples [22], a smooth variation of k_{uni} versus E is observed. We also note that the rate on the first step is roughly 1/2 and 1/3 of the rates on the second and third steps, respectively.

4. Discussion

The simplest form of microcanonical transition state theory uses eq. (3) to compute the unimolecular decomposition rate, $k_{\mathrm{uni}}(E)$

$$k_{\mathrm{uni}}(E) = \frac{N^*(E-E_0)}{h\rho(E)}\,, \qquad (3)$$

where $N^*(E-E_0)$ is the number of accessible states of the transition state at energy E without inclusion of the reaction coordinate, E_0 is the reaction thresh-

old, which in the present case is taken to be the same as D_0 since rotation is minimal and there is no reverse barrier, and $\rho(E)$ is the density of states of the parent molecule. $N^*(E-E_0)$ can be estimated at a single transition state in the simplest applications of eq. (3), or at transition states obtained variationally to satisfy a minimum flux criterion.

The view embodied in eq. (3) can predict rates with uncanny success. $N^*(E-E_0)$ rises in steps, taking on the value unity just above threshold when only one internal level of the transition state is accessible. With increasing energy, N^* changes from 1 to 2 when two channels become available, and so on. Since $\rho(E)$ changes more slowly than $N^*(E)$, eq. (3) predicts a step-like increase of k_{uni} with energy. For large molecules having many internal degrees of freedom the step-like behavior will generally be too fine-grained to be observed except in the most sophisticated experiments, while for small molecules it may be more easily observed. It is tempting to consider the possibility that the measured k_{uni} values shown in fig. 3 can be rationalized in terms of eq. (3): For example, is the step-like behavior a manifestation of $N^*=1$, 2, etc.?

Although reaction via S_0 character is assured, NO_2 does not fit comfortably into the niche of standard unimolecular decomposition models. It has a complex electronic structure that derives from the conical intersection between the $^2A_1$ ground and $^2B_2$ excited states; it is a triatomic with a modest density of states in the threshold region; reaction rates are rapid and may compete with intramolecular vibrational redistribution, which is not even easy to define for so small a system; etc. Furthermore, because of the modest density of states and the fact that our measurements do not include a large number of levels, statistical fluctuations in the rates may occur [21]. The above considerations notwithstanding, it is still interesting to compare $k_{uni}(E)$ from eq. (3) to the data.

Fortunately, it is possible to obtain experimentally based estimates of vibronic and rovibronic state densities for NO_2 in the region just below D_0. For example, Delon et al. recently examined NO_2 spectra in great detail in the region 16500–18500 cm^{-1}. They observed 159 vibronic B_2-symmetry levels of the strongly mixed $^2B_2$ and $^2A_1$ electronic states in this interval [4]. By extrapolating from observed levels in the region 0–10000 cm^{-1} [3], they deduced that there are most likely 210 levels in the 16500–18500 cm^{-1} interval. Taking this level density of ≈ 0.1 per cm^{-1}, and extrapolating to D_0 by assuming that the density increases as $(E+E_{00})^2$ [23], where $E_{00}=1844$ cm^{-1} is the NO_2 zero-point vibrational energy, yields a level density of ≈ 0.2 per cm^{-1} near D_0. Substituting this into eq. (3) with $N^\ddagger=1$ yields 1.5×10^{11} s^{-1} for the threshold rate. Thus, if the vibronic level density measured by Delon et al. is extrapolated to D_0, the step-like k_{uni} variation observed experimentally can be assigned to the opening of channels at the transition state.

A more precise evaluation of the near threshold density of NO_2 rovibronic states may be obtained from recently reported LIF spectra which have been recorded for 1 K expansion cooled samples having 98% of the NO_2 molecules in the lowest rotational level. Under these experimental conditions, Miyawaki et al. observe more than 60 transitions in the 25 cm^{-1} region immediately below D_0 [9]. Since $J=1/2$ for the lowest rotational level, the one-photon electric dipole excitation process carries molecules to $J=1/2$ and $3/2$, each of which contributes to the observed density of spectral lines. It should be mentioned that the "observed" levels are obtained from visual inspection of a published spectrum and, as a result of limited resolution, there may be additional levels that do not show up; also, some of the small peaks may originate from levels other than $J=1/2$. Other groups have also reported highly structured spectra below D_0 [7] which are in general agreement with the Miyawaki et al. results. Above D_0, lifetime broadening results in overlap of zeroth-order levels, making it impractical to recover level densities from absorption spectra.

It is clear from the spectroscopic results of Miyawaki et al. that the observed level density near D_0 is higher than that obtained by extrapolation of the vibronic level density. The difference is most likely due to spin-rotation and Coriolis couplings. For example, if $J=1/2$ and $3/2$ are produced by one-photon absorption from the $J=1/2$ ground state, we anticipate six rotational sublevels for each vibronic level [22]. Since rotational degeneracies of vibronic levels enter both the numerator and denominator of eq. (3), $\rho(E)$ and $N^*(E-D_0)$ can be interpreted either as the density and number of rovibronic levels

for given J and E or as those for vibronic levels, without affecting the final result. Thus, the Miyawaki et al. data are consistent with a vibronic level density of ≈ 0.4 per cm^{-1}, which is close to the extrapolated Delon et al. value of ≈ 0.2 per cm^{-1}. Both estimations are consistent with a simple interpretation of the steps in $k_{uni}(E)$ in terms of transition state levels corresponding to $N^* = 1,2$, etc.

In experiments carried out by Moore and co-workers using expansion-cooled CH_2CO, step-like rises in the yield for the singlet channel were observed with energy increments corresponding to CO rotational levels [24,25]. These steps may be due to competition between singlet and triplet exit channels past a rate-limiting transition state. With our experimental resolution, steps of such small increments could not be resolved even if the NO_2 spectral features were more continuous. However, if such small steps were present, they would manifest themselves at our resolution as a monotonic rise in k_{uni} versus E, which is not the case. Zewail and co-workers, on the other hand, measured rates for CH_2CO decomposition [20] which were reconciled using the variational RRKM approach espoused by Marcus and co-workers with transition state parameters that include low frequency vibrations [26]. Also, in the experiments of Zewail and co-workers on NCNO decomposition, it was shown that the rates increased smoothly with energy except near 320 cm^{-1}, where structure in the $k(E)$ versus E curve was clearly discerned [19]; again, a variational RRKM analysis employed low-frequency vibrations at the transition state [27].

The observed spacings of ≈ 100 cm^{-1} for NO_2 are a bit high in light of the above detailed studies of small molecules decomposing via loose transition states [19,20,24–27]. These spacings may correspond either to transition state levels that correlate with atomic oxygen $^3P_2$, $^3P_1$, and $^3P_1$ fine-structure levels, which are at 0, 158 and 227 cm^{-1}, respectively, in the free atom [28]; or alternatively to a bending frequency at the transition state. Since the first interpretation implies a low frequency bend or rotor at the transition state, resulting in a monotonic rise which is not observed, we favor the latter interpretation. The conical intersection between $^2A_1$ and $^2B_2$ may also play a role, since it lies near the exit channel and zeroth-order $^2B_2$ does not dissociate to ground electronic state products. Thus, the $^2B_2$ part of the wavefunction lends "tight transition state" character to the overall wavefunction, so the steps may reflect passage through the region of conical intersection. Such passage from one region of bound potential to another has been clearly demonstrated by Zewail and co-workers in the NaI system [31].

At the energies accessed in the present experiments, the transition state involves only one "vibration" since the NO-stretch is too energetic, i.e. 1876 cm^{-1} for free NO [29]. Thus, evaluating $N^*(E-E_0)$ is a matter of choosing the bend frequency and counting open channels. The rate in the region 0–100 cm^{-1} can then be attributed to a vibrationless transition state having $N^* = 1$. The rise near 100 cm^{-1} is associated with $v = 1$ of the bend, and likewise the step near 200 cm^{-1} is associated with $v = 2$. This is consistent with the approximate 1:2:3 ratio of the relative rates on the first, second and third steps. Finally, we note that steps are only evident to ≈ 350 cm^{-1}. Two explanations may be offered: (i) deteriorating experimental accuracy past ≈ 350 cm^{-1} hides details of the $k_{uni}(E)$ dependence, and (ii) the pattern may change, for example because of a transition from bending to internal rotation. Such questions are left for further investigations.

In summary, NO_2 photoexcited above D_0 undergoes unimolecular decomposition due to its ground electronic state character. With expansion-cooled samples, k_{uni} versus E is not smooth, but shows step-like behavior that can be reconciled with RRKM theory, using experimental densities of states. Much remains to be done with this most unusual system.

Acknowledgement

The authors acknowledge many useful discussions with H. Reisler, D.C. Robie, M. Hunter, and A.H. Zewail.

References

[1] R.E. Smalley, L. Wharton and D.H. Levy, J. Chem. Phys. 63 (1976) 4989.
[2] S. Hiraoka, K. Shibuya and K. Obi, J. Mol. Spectry. 126 (1987) 427.
[3] A. Delon and R. Jost, J. Chem. Phys. 95 (1991) 5686.

[4] A. Delon, R. Jost and M. Lombardi, J. Chem. Phys. 95 (1991) 5700.
[5] H. Zacharias, M. Geilhaupt, K. Meier and K.H. Welge, J. Chem. Phys. 74 (1981) 218.
[6] H. Zacharias, K. Meier and K.H. Welge, in: Energy storage and redistribution in molecules, ed. J. Hinze (Plenum Press, New York, 1983) p. 107.
[7] U. Robra, H. Zacharias and K.H. Welge, Z. Phys. D 16 (1990) 175.
[8] J. Miyawaki, T. Tsuchizawa, K. Yamanouchi and S. Tsuchiya, Chem. Phys. Letters 165 (1990) 168.
[9] J. Miyawaki, K. Yamanouchi and S. Tsuchiya, Chem. Phys. Letters 180 (1991) 287.
[10] D.C. Robie, M. Hunter, J.L. Bates and H. Reisler, to be published.
[11] C.F. Jackels and E.R. Davidson, J. Chem. Phys. 64 (1976) 2908.
[12] C.F. Jackels and E.R. Davidson, J. Chem. Phys. 65 (1976) 2941.
[13] C.H. Chen, D.W. Clark, M.G. Payne and S.D. Kramer, Opt. Commun. 32 (1980) 391.
[14] G.E. Busch and K.R. Wilson, J. Chem. Phys. 56 (1972) 3538.
[15] H. Gaedtke, H. Hippler and J. Troe, Chem. Phys. Letters 16 (1972) 177.
[16] M. Quack and J. Troe, Ber. Bunsenges. Physik. Chem. 78 (1974) 240.
[17] D.M. Wardlaw and R.A. Marcus, J. Chem. Phys. 83 (1985) 3462.
[18] B.M. Toselli and J.R. Barker, J. Chem. Phys. 91 (1989) 2239.
[19] L.R. Khundar, J.L. Knee and A.H. Zewail, J. Chem. Phys. 87 (1987) 77.
[20] E.D. Potter, M. Gruebele, L.R. Khundar and A.H. Zewail, Chem. Phys. Letters 164(1989) 463.
[21] W.F. Polik, D.R. Guyer and C.B. Moore, J. Chem. Phys. 92 (1990) 3453.
[22] S.I. Ionov, G.A. Brucker, Y. Chen, C. Jaques and C. Wittig, unpublished.
[23] R.A. Marcus and O.K. Rice, J. Phys. Colloid Chem. 55 (1951) 894.
[24] I.-C. Chen, W.H. Green and C.B. Moore, J. Chem. Phys. 89 (1988) 314.
[25] W.H. Green, A.J. Mahoney, Q.-K. Zheng and C.B. Moore, J. Chem. Phys. 94(1991) 1961.
[26] S.J. Klippenstein and R.A. Marcus, J. Chem. Phys. 91 (1989) 2280.
[27] S.J. Klippenstein, L.R. Khundar, A.H. Zewail and R.A. Marcus, J. Chem. Phys. 89 (1988) 4761.
[28] S. Bashkin and J.O. Stoner Jr., Atomic energy levels and Grotrian diagrams, Vol. 1 (North-Holland, Amsterdam, 1975).
[29] G. Herzberg, Molecular spectra and molecular structure, Vol. 1 (Van Nostrand, Princeton, 1950).
[30] G. Herzberg, Molecular spectra and molecular structure, Vol. 3 (Van Nostrand, Princeton, 1966).
[31] A.H. Zewail, Faraday Discussions Chem. Soc. 91 (1991) 207.